Lalpoor, M.; Miroux, A.; Mendis, C.L.; Hort, N.; Offerman, S.E.:

The interaction of precipitation and deformation in a binary Mg–Ca alloy at elevated temperatures

In: Materials Science and Engineering A (2014) Elsevier

DOI: 10.1016/j.msea.2014.04.095

The interaction of precipitation and deformation in a binary Mg-Ca alloy at elevated temperatures

M. Lalpoor [a,b], A. Miroux [a,b], C.L. Mendis [c], N. Hort [c], S.E. Offerman [a]

[a] *Delft University of Technology, Department of Materials Science and Engineering, Mekelweg 2, 2628 CD Delft, The Netherlands*

[b] *Materials innovation institute, Mekelweg 2, 2628 CD Delft, The Netherlands*

[c] *Magnesium Innovation Center, Helmholtz Zentrum Geesthacht, Max-Planck-Straße 1 21502 Geesthacht, Germany*

Corresponding author: Mehdi Lalpoor, Delft University of Technology, Department of Materials Science and Engineering, Mekelweg 2, 2628 CD Delft, The Netherlands. Email: mlalpoor@gmail.com

The effect of pre-deformation on precipitation hardening response as well as the work-hardening behavior of a binary Mg-Ca alloy is investigated. Our results show that application of 5% pre-deformation increases the precipitation hardening response of the material and decreases the annealing time by 50%. The dislocations introduced during the pre-deformation process act as predominant nucleation sites and result in a higher number of precipitates of smaller size. During the thermomechanical treatments, the work hardening behavior is altered by the state of the precipitates, namely under-aged, peak-aged and over-aged. After the elastic-plastic transition, under-aged and peak-aged materials show a continuously decreasing work-hardening rate, while the over-aged material has an initial constant work-hardening rate. The absolute values of the work hardening rate are far less sensitive to the precipitation stage compared to aluminum alloys; a fact that explains the low work hardening capacity of magnesium compared to aluminum.

Introduction

Up to three billion more middle class consumers will emerge in the next 20 years compared with the current 1.8 billion driving up demand for a range of resources [1]. Bridging such a gap in materials production sounds like a challenge for materials science and related industries. The alloying elements with a key role in industrial alloys seem to become more and more scarce and their replacement with abundant elements does not seem to be very straight forward. Magnesium alloys are sensitive to the scarcity of crucial elements, since their strength, ductility and creep resistance are obtained mainly through alloying with rare-earth (RE) elements, or other critical elements such as Zn, Zr or Sr [2-4]. The lack of plasticity at room temperature, a direct consequence of the *hcp* crystallographic structure, limits the possibility of strengthening of Mg-alloys by cold working [3, 5]. This explains the significant role of alloying elements in strengthening of Mg alloys, and has driven the development of Mg alloys in the direction of cast-products [3]. In the situation of limited availability of RE and critical alloying elements, abundant elements such as Al, Ca and Si along with other strengthening

mechanisms such as precipitation hardening and grain size reduction should be used to improve the mechanical properties of Mg alloys to a level allowing practical applications. However, there are two main drawbacks in development of precipitation hardenable wrought magnesium alloys, namely the low precipitation hardening response and the lack of knowledge on thermomechanical behavior.

The precipitation hardening response of Mg-Al and Mg-Ca alloy systems is rather low and supplementary treatments are required to improve it [6-8]. Three known approaches are: step aging [9], addition of trace amount of ternary or quaternary elements (micro-alloying) [6, 10, 11], or application of slight amount of pre-deformation. Step aging is tried for AZ91 alloy, however it is known to be effective when GP zones form prior to equilibrium precipitates (as in Mg-Zn system [12]), which is not the case for precipitation of $Mg_{17}Al_{12}$ from super saturated solid solution [3]. Regarding the micro-alloying, the exact mechanism of which is not fully understood, although it results in significant increase of hardness it fails in reducing the annealing time considerably. By the way, the trace elements used to increase the precipitation hardening response are getting more scarce and expensive (Ag, Zr, and RE [4]). Considering the last technique, although it is already known that introduction of dislocations to the structure may enhance the precipitation hardening response of a single crystalline Mg alloy [13, 14], a systematic work has not been performed on a poly crystalline alloy to study this phenomenon quantitatively. In a former study on nucleation of $Mg_{17}Al_{12}$ precipitates [8], present authors found that application of small amount of deformation prior to aging, may accelerate the nucleation by introducing dislocations or twin bands to the structure. Therefore, it would be interesting to know how pre-deformation affects the precipitation hardening response in such alloys with the aim to search for sustainable methods of materials production in the absence of scarce or expensive elements. As a case study, the Mg-Ca system has been selected for this investigation.

The other drawback in development of wrought Mg alloys with controlled microstructure, is the lack of knowledge on their thermomechanical behavior. Limited work focuses on the traditional wrought AZ31 alloy [15, 16] and the precipitation hardenable ZK60 alloy [17, 18]. While the general warm deformation and recrystallization behavior is addressed in these studies, the role of precipitation in controlling the thermomechanical behavior is not considered. On the one hand dealing with precipitates is inevitable during the thermomechanical treatment of precipitation hardenable systems, as substantial amount of deformation in Mg alloys is achievable only at elevated temperatures. On the other hand, the interaction of precipitation and deformation depends on the nature and type of precipitates and varies from one system to the other. This is also true for Mg alloys containing abundant elements such as Al and Si or for the Mg-Ca system which is of interest for this study. Precipitation in Mg-Ca alloys has already been studied. Binary Mg-Ca alloy form prismatic Mg_2Ca precipitates with a polygonal shape on the basal plane and facets along {1 0 -1 0} plane [10]. Their size is typically several tens of nanometers. Large lattice misfit with the Mg matrix is expected due to the large atomic radius of Ca (1.97 Å) compared to Mg (1.60 Å) [11]. The nature of the precipitates can, however, drastically change with the introduction of an additional alloying element like Al [11] or

Zn [19]. A high density of fine GP zones form during ageing of these ternary alloys instead of the coarse Mg_2Ca. These GP zones are plates lying on the basal plane, with a thickness of 1 or 2 atomic layers and length smaller than 10 nm. The high density of GP zones is responsible for the strength increase compared to the binary Mg-Ca alloy. While Mg-Ca alloys have been traditionally used for creep applications [20, 21], they have recently attracted more attention for wrought purposes [22]. However, no results have been published on thermomechanical behavior of such alloys. Therefore, it is essential to understand and quantify the role of precipitation in plastic deformation and work hardening behavior at elevated temperatures. Special thermomechanical treatments need to be designed for this purpose. The work hardening and dynamic recovery rates determined through thermomechanical treatments may help us understand and control the thermomechanical processes.

The aim of our work is therefore neither to develop a new alloy nor generate superior properties, but to bridge the knowledge gap on thermomechanical behavior of Mg-Ca alloys and to investigate the influence of pre-deformation on ageing process. The novelty and originality of the current work lies in considering the role of precipitation in thermomechanical processing; a study which has not been performed in Mg-alloys.

Experimental procedure

The material selected for this study is a Mg-1 wt.% Ca alloy produced by indirect chill permanent mold casting. The as-cast micro-structure includes grains of α-Mg phase surrounded by eutectic patches of $\alpha+Mg_2Ca$. In order to homogenize the distribution of Ca in the α-Mg matrix, the material is heated in a steel envelope at 480 °C for 6 h and then quenched in water. Experiment is designed as shown in Fig. 1a to understand the effect of pre-deformation on precipitation hardening response of our material. For the material without pre-deformation, the homogenization treatment is followed by annealing at 250°C for various times namely, 5, 10, 15, 30 min and 1, 2, 3, 5, 8, 10, 12 and 16.5 h. Similar treatment is applied to the material after 1, 2 and 5% uniaxial compression at the strain rate of 10^{-3} s^{-1} and at 100 °C, and the results are compared to the non-deformed material. Micro-hardness tests are performed using the Struers-Dura Scan 70 machine with an indentation load of 100 g. 40 indentations are done for each case in grids of 4×10 points 200 μm away from each other, and the average values are reported. Thus, an area of 1.1 mm^2 is covered in order to assure the statistical reliability of the data.

In order to understand how temperature and precipitates influence the thermomechanical behavior of the material, several experiments are designed. Three initial materials containing different populations of precipitates are produced taking advantage of the knowledge of the ageing process. The first is the over-aged stage (Fig. 1b), the second one peak-aged (Fig. 1c) and the last one under-aged (Fig. 1d). To

make over-aged samples, the material is annealed at 250 °C for 1 h* followed by uniaxial compression for 30% at three different temperatures namely 250, 300 and 350 °C, which are the typical thermomechanical treatment temperatures of Mg-alloys. In the case of peak-aged samples, the material is first pre-deformed (uniaxial compression at the strain rate of 10^{-3} s^{-1}) for 5% at 100°C, followed by precipitation hardening treatment at 250 °C for 5 minutes and finally 30% uniaxial compression at 250, 300 and 350 °C. For the under-aged condition, the as-homogenized material is uniaxially compressed up to 30% at 250 °C. The term "under-aged" is used to account for the heating interval (30 s) and the holding time (10 s) at 250 °C before the deformation starts.

All thermomechanical treatments are performed in Gleeble 1500 under protective Argon atmosphere and strain rate of 10^{-3} s^{-1}. Cylindrical specimen (10 mm in diameter and 12 mm long) are heated through Joule effect at the rate of 10 °C/s and quenched after the end of treatment by a jet of Nitrogen. To reduce the friction effect, graphite flakes are used at both contact points of the compression specimens and hydraulic jaws. 2 samples are tested for each condition and the average values are reported here.

The polarized light Neophot 30 optical microscopy is used for investigation of the microstructure and grain size measurement. After grinding and polishing, samples are etched in the Acetic-picral solution: (5 mL acetic acid, 6 g picric acid, 10 mL H_2O, 100 mL ethanol (95%)). The average grain size was measured based on ASTM Standard E112 method [23].

In order to investigate the role of precipitates in plastic deformation, and the effect of pre-deformation on precipitation transmission electron microscopy (TEM) experiments are performed on the heat-treated samples. The samples for TEM work were prepared by electron discharge machining 3mm diameter discs from strips of alloy cut to a thickness of 200 μm using a slow speed cutter (Isomat Slow speed cutter) to prevent additional deformation. The samples were electropolished in a Fishione Twin Jet electropolisher with a solution consisting of 1.5 vol.% Perchloric acid in ethanol at a polishing temperature of -45 $^{\circ}$C and a voltage of ~90 V. The samples were examined with a FEI CM200 transmission electron microscope operating at 200 kV.

Results and discussion

1. Precipitation hardening and the effect of pre-deformation

The microstructure of the sample in the as-homogenized state is shown in Fig. 2. It has an average grain size of 73.9 ± 6.3 μm. Fig. 3a shows the evolution of hardness in Mg-1 wt.% Ca alloy during precipitation hardening treatment at 250 °C for various times. As can be seen, in the non-deformed material a peak of hardness is reached after 10 minutes (600 s), but the hardness falls afterwards and

* The time required for over-aging the alloy was determined from the preliminary hardness tests, the results of which are shown in more details in the next section.

remains roughly constant after 1 h (3600 s) (the results are not shown after 3 h). These results are consistent with previous observations in Mg-Ca alloys [11, 19, 20] where the low aging response of such alloys is reported. We observed in early works on Mg-Al that twinning bands forming during sample preparation can act as nucleation sites for $Mg_{17}Al_{12}$ precipitates in a binary Mg-7 wt.% Al alloy [8]. However, it has not been studied systematically how slight amount of pre-deformation can increase the aging response of Mg alloys. Our results indicate that 5% deformation at 100 °C results in 14% increase of peak hardness and 50% reduction of the time required to reach the maximum (Fig. 3b). The reason for this behavior may be better understood if we compare the TEM images of the samples precipitation hardened without and with pre-deformation (Figs. 4a and b respectively). Fig. 4a shows the structure of the material (treated at 250 °C for 5 min) without any pre-deformation, and Fig. 4b the peak aged one (treated at 250 °C for 5 min) with 5% pre-deformation. As can be seen in Fig. 4b, the pre-deformation has stimulated the precipitation of Mg_2Ca on dislocations, which act as preferential nucleation sites. The finer dispersion of the precipitates along with strain hardening at 100 °C is responsible for the increased hardness observed at the lower aging time of 5 min. Introducing dislocations to the structure increases the number and decreases the average size of precipitates (from 52.0 ± 2.2 nm in non-deformed sample annealed for 5 min (Fig. 4a) to 35.9 ± 2.8 nm in the sample with 5% pre-deformation annealed for 5 min (Fig. 4b)). Although the increase in hardness is also observed in samples deformed for 1 and 2%, the 5% deformation appears to be the threshold for significant stimulation of precipitation by dislocations.

While the increase in hardness sounds insignificant compared to micro-alloying, the application of pre-deformation has two main advantages over micro-alloying. The first is that there is no need to add scarce or critical elements such as Ag, Zr, etc. The other advantage is the 50% reduction in the annealing time needed to reach the peak hardness, which reduces the energy consumption of the process. By the way, there is a chance to improve this technique by changing the mode (to tensile or shear), and/or tuning the amount, temperature and rate of pre-deformation. A comparison with step aging is not possible, as this technique would be useful only for ternary Mg-Ca systems, where GP zones form.

2. Stress-true strain curves and mechanical properties at elevated temperatures

Following the hardness investigations, thermomechanical experiments were performed on samples with precipitates in various states, namely over-aged (aged for 1 h at 250 °C), peak-aged (pre-deformed for 5% at 100°C, followed by aging at 250 °C for 5 min) and under-aged (as-homogenized). The results of the thermomechanical treatments are shown in Figs. 5a through c. Stress-true strain curves show that the material exhibits different work hardening behaviors in different precipitation hardening stages. The serrations observed in Fig. 5a are due to the higher data acquisition rate chosen for these samples. The yield and ultimate compressive strength of the alloys investigated are shown in

Figs. 6a and b. As can be seen, at 250°C, the peak-aged alloy shows the highest yield strength of the three conditions. This behavior can be explained by the fact that the highest density of precipitates in the peak-aged material provides the highest resistance against the dislocation movement in this alloy and results in the highest yield strength. However, the difference in yield strength between the peak-aged and over-aged alloys diminishes with increase of deformation temperature. This indicates that the precipitates contribution to the yield strength decreases with increasing the deformation temperature. At all deformation temperatures, the ultimate compressive strength hardly depends on the precipitation stage. As expected, the ultimate compressive strength decreases with increasing temperature.

3. Work hardening behavior

In order to investigate the work hardening behavior of the material, the θ - $(\sigma-\sigma_y)$ plots ($\theta = d\sigma/d\varepsilon$) are generated from Fig. 5. The σ_y defined here is the proportionality limit beyond which the linearity between stress and elastic strain is not valid any more. Figs. 7a through c show the changes in the work hardening rate ($\theta = d\sigma/d\varepsilon$) versus $(\sigma-\sigma_y)$ for the Mg-1Ca alloy at different precipitation stages. As can be seen, for the over-aged material at 250 and 300°C, there is a plateau after a sharp fall in the work hardening rate. The sharp fall in work hardening rate corresponds to the elastic-plastic transition, after which, the work hardening rate remains constant until another drop is observed at higher stresses. Such a behavior has been observed in over-aged AA 6005A-T6 Aluminum alloys [24]. For the peak-aged material, after the elastic-plastic transition, there is a sharp decrease in the absolute value of the slope when entering the stage III of plastic deformation [25], but no plateau is observed here and the work hardening rate keeps on decreasing with stress (Fig. 7b). A similar trend is observed for the under-aged alloy (Fig. 7c) although the transition from the elastic-plastic to the stage III work-hardening regime is less sharp compared to over-aged and peak-aged alloys (Figs. 7a and b).

3.1. θ_0 and β *vs.* yield stress

From Figs. 7a through c, one may determine the initial work hardening rate at the onset of stage III, θ_0, and the dynamic recovery rate during stage III ($\beta = -d\theta/d\sigma$). The dashed guidelines show schematically how θ_0 is determined from the curves. For the peak-aged as well under-aged conditions, tangent lines are drawn to curve wings and the intersection points are recorded as θ_0. For the over-aged condition a tangent line to the horizontal linear part of the curve determines the θ_0. To illustrate the dependence of these two parameters on the precipitation stage, we plot them versus the yield strength. The results for the analysis of the initial work-hardening rate as a function of the yield stress (proportionality limit) during compression at 250 °C are shown in Fig. 8a. It can be observed that as the yield stress first increases during aging, the initial work-hardening rate increases to a maximum

near the peak strength. Once over-aged, the yield stress decreases below 45 MPa and θ_0 dramatically falls. Fig. 8b shows the changes of β in samples with various precipitation states. β shows its highest value in under-aged condition followed by a drop to reach a minimum in peak-aged and then another increase in over-aged condition. The study of work hardening behavior in precipitation hardenable AA6111 and AA7030 aluminum alloys [26] has shown that the initial work hardening rate (θ_0) is maximum for the solution heat treated material (~2250 MPa in AA6111) and decreases to a minimum (~750 MPa in AA6111) near the peak strength. There is then a constant or slightly increasing value for θ_0 as the yield stress drops during over-aging. Once the over-aged yield stress drops below a certain value, θ_0 dramatically increases (up to ~1900 MPa in AA6111) before decreasing again for long over-aging times. The value of β is almost constant up to the peak strength with a magnitude of 12.5 to 15 (in AA6111). Again, at a certain yield stress, the magnitude of β increases dramatically and then remains constant at a value of 35 to 40 (in AA6111). Comparing the behavior of the Mg-Ca with aluminum alloys, one learns that the absolute initial work hardening rates observed in Fig. 8a (~500 MPa in under-aged, ~531 MPa in peak-aged and ~425 MPa in over-aged condition) are much lower compared to precipitation hardenable AA6111 and AA7030 aluminum alloys, which explains the poor work hardening capacity of the magnesium alloy under discussion.

3.2. TEM observations

TEM investigation of the under-aged, peak-aged and over-aged samples after 30% compression at 250°C aims to clarify the possible work-hardening mechanisms of the Mg-Ca alloy. Figs. 9a through c show that the highest density of precipitates (having an average precipitates diameter = 33.1 ± 1.8 nm) appears in the peak-aged material. In under-aged material, precipitates are hardly detectable and in the over-aged they have coarsened considerably (having an average precipitates diameter = 50.7 ± 2.9 nm) compared to peak-aged condition. Unfortunately, it is not clear whether the precipitates are sheared and to detect this requires high resolution TEM analysis and a detailed study of the precipitates habit planes and possible slip systems at corresponding temperatures, which remains a topic for further research. However, no mechanical twinning was observed at 250°C for all conditions and at this temperature, the main deformation and recovery mechanisms are expected to be dislocation glide, cross-slip and climb [17].

TEM images revealed that very limited dynamic precipitation takes place during compression of the under-aged sample (Fig.9a) and therefore the content of Ca in solid solution should remain close to the one after homogenization (0.56 wt.% according to equilibrium thermodynamic calculations by Thermo-Calc Software). Alloying elements in solid solution in Mg alloys can significantly influence the stacking fault energy and the relative critical resolved shear stress of the different slip systems [27]. However, not all elements have the same effect and no information is available on the effect of Ca. Therefore, further study would be required to determine the precise effect of Ca in solid solution

on dislocation storage and recovery. On the contrary, the amount of Ca in solid solution in the peak-aged material is expected to be minimum (~0.07 wt.% according to equilibrium thermodynamic calculations by Thermo-Calc Software) for a fine distribution of precipitates. Assuming that the lower solute content in peak-aged condition should decrease θ_0 compared to under-aged as in aluminum alloys [26], the slight increase of θ_0 observed in the compression test results of Mg-1 wt.% Ca alloy (Fig. 8a) suggests that the precipitates in the peak-aged material contribute to the storage of dislocations. Since shearable precipitates have limited influence on dislocation storage [24, 26] the precipitates formed in peak-aged condition are probably non-shearable. The measured size of the precipitates remains the same before and after 30% compression at 250°C, 35.9 ± 2.8 and 33.1 ± 1.8 nm respectively, which is consistent with a by-pass mechanism. Similar increase of the initial work-hardening rate due to the formation of precipitates has been observed at room temperature in alloy AZ91 and was also interpreted as the consequence of a by-pass mechanism by cross slip [28]. On the contrary, Chen et al. [29] observed for the alloy ZK60 that peak-aged material has a lower initial room temperature work-hardening rate than the under-aged material, as in aluminum alloys in which most of precipitates at peak-aged condition are shearable [30]. The effect of precipitates on the work-hardening of Mg alloys is, therefore, strongly dependent on the nature of the precipitates. The lower solute content in peak-aged condition should also facilitate dynamic recovery (higher β) compared to under-aged condition. The observed decrease of β from under-aged to peak-aged samples (see Fig. 8b) indicates that precipitates also hinder the dynamic recovery process. This is confirmed by TEM images showing better defined dislocation cell structure in the under-aged sample than in the peak-aged sample (Figs. 10a and b).

The decrease of θ_0 and increase of β from peak-aged to over-aged condition is due to precipitate coarsening since Ca solute content is expected to be minimum in both conditions. Therefore, the contribution of precipitates to dislocation storage and on retarding dynamic recovery decreases when the precipitate density decreases. A plateau in θ - $(\sigma - \sigma_y)$ curve after the elastic-plastic transition is observed during compression at 250 and 300°C of the over-aged specimens. Similar plateau in the work-hardening plot has been observed at room temperature for ZK60 alloy containing $MgZn_2$ precipitates [31], for over-aged aluminum alloys [26] as well as during the room temperature deformation of AZ31B-H24 alloy containing a high initial density of forest dislocations [32]. This constant initial work-hardening rate corresponds to a regime of planar glide on the basal plane with pile-up of dislocations on or accumulation of dislocation loops around strong obstacles, either non-shearable precipitates or forest dislocations, which delays the onset of dynamic recovery and leads to a linear hardening regime or stage II [33, 34]. This regime finishes when glide on basal plane becomes too difficult and non-basal systems become active. The presence of stage II for the over-aged material (Fig. 7a) and its absence in peak-aged material (Fig. 7b) might be related to the relative spatial distribution of precipitates and dislocations; in the over-aged material precipitates are randomly

distributed in an initially undeformed material, and consequently glide of dislocations and accumulation of dislocation loops around precipitates is supposed to be the dominant mechanism at the beginning of plastic deformation, which gives a constant θ. Precipitates in the peak-aged material have formed directly on the dislocations introduced during 5% pre-deformation (Fig. 4b) and should immediately oppose a large resistance to dislocation glide on the basal slip system. Cross-slip might be very quickly activated and contribute to the redistribution of dislocation in the volume and to dynamic recovery, decreasing the work-hardening rate from the beginning of stage III.

3.3. θ_0 and β *vs.* temperature

Figures 11a and b show the temperature dependence of the initial work hardening rate, θ_0, and the dynamic recovery rate β. For the peak-aged as well as over-aged alloys, θ_0 decreases with increasing temperature. Since the dislocation storage in these two materials is supposed to be mainly controlled by the interaction with precipitates, increasing the deformation temperature will facilitate cross-slip and dislocation climb, making it easier for the dislocations to overcome the precipitates, and reduce the initial work hardening rate. For the over-aged samples treated at 350 °C, the work hardening rate decreases down to zero without any change of slope (as observed in Figs. 5a and 7a) and no work-hardening parameter could be determined for this condition. The change in the dynamic recovery rate with temperature is shown in Fig. 11b and it can be seen that for both peak-aged and over-aged materials, the β increases with an increase in deformation temperature. Since dynamic recovery is a thermally activated process, the ease of dislocation annihilation at elevated temperatures describes this behavior [35]. The rate of changes in θ_0 and β with temperature is different for peak-aged and over-aged conditions, a fact that appeals further investigations.

Conclusions

The effect of pre-deformation on precipitation hardening response of a binary Mg-Ca alloy was investigated. In line with previous observations in other Mg-alloys, the aging response of the Mg-1 wt.% Ca alloy is low and the coarsening of the precipitates results in a drop after reaching the peak-aged hardness. Our results show, however that the low aging response of the Mg-Ca alloy can be improved by slight amount of pre-deformation: 5% pre-deformation at 100 °C results in 14% increase of peak hardness and 50% reduction of the aging time. The increased hardness is a direct consequence of stimulated nucleation of precipitation on dislocations formed during the pre-deformation. Introducing dislocations to the structure results in higher number precipitates of smaller size. While the increase in peak hardness sounds insignificant compared to micro-alloying, this sustainable method may still be a potential way to replace addition of trace elements (such as Zn [10]) to Mg-Ca alloys

with the aim to improve the precipitation hardening response. Reduction of the annealing time by 50% and no need to add expensive scarce elements justifies future investigation on this method.

Concerning the thermomechanical behavior, our results show that although the peak-aged alloy results in the highest yield strength during the deformation process, the under-aged material yields a medium yield and ultimate compressive strength similar to the other conditions. The yield strength of the alloy is more sensitive to the population of precipitates than the ultimate compressive strength. Regarding the work hardening behavior, after the elastic/plastic transition, two distinctive types of behavior are observed. For under-aged and peak-aged samples, there is an approximately linear decrease of work-hardening rate as the flow stress increases. For the over-aged samples, after the elastic/plastic transition, the work hardening rate shows an almost constant hardening rate followed by a sharp decrease in hardening rate as the flow stress increases. Precipitates appear to promote dislocation storage and hinder dynamic recovery such that work-hardening rate is maximum and dynamic recovery rate is minimum for material in peak-aged condition. The absolute values of the work hardening rate are far less sensitive to the precipitation stage compared to precipitation hardenable aluminum alloys; a fact that explains the low work hardening capacity of the Mg-Ca alloy.

Acknowledgments

This research was carried out under the project number M42.5.10395 in the framework of the Research Program of the Materials innovation institute M2i (www.m2i.nl).

References

[1] R. Dobbs, J. Oppenheim, F. Thompson, M. Brinkman, M. Zornes, McKinsey Global Institute, 2011.

[2] S.K. Das, L.A. Davis, Materials Science and Engineering, 98 (1988) 1-12.

[3] I.J. Polmear, Materials Science and Technology 10 (1994) 1-16.

[4] K. Hono, C.L. Mendis, T.T. Sasaki, K. Oh-ishi, Scripta Materialia 63 (2010) 710–715.

[5] B.L. Mordike, T. Ebert, Materials Science and Engineering A, 302 (2001) 37–45.

[6] S. Celotto, Acta Materialia, 48 (2000) 1775-1787.

[7] J.F. Nie, Metallurgical and Materials Transactions A, 43 (2012) 3891-3939.

[8] M. Lalpoor, J.S. Dzwonczyk, N. Hort, S.E. Offerman, Journal of Alloys and Compounds 557 (2013) 73–76.

[9] A.F. Crawley, B. Lagowski, Metallurgical Transactions 5(1974) 949-951.

[10] K. Oh-ishi, R.Watanabe, C.L. Mendis, K. Hono, Materials Science and Engineering A 526 (2009) 177–184.

[11] J. Jayaraj, C.L. Mendis, T. Ohkubo, K. Oh-ishi, K. Hono, Scripta Materialia 63 (2010) 831–834.
[12] K. Oh-ishi, K. Hono, K.S. Shin, Materials Science and Engineering A 496 (2008) 425–433.
[13] R.D. Luca, J.G. Byrne, Acta Metallurgica, 13 (1965) 1187-1195.
[14] R.D. Luca, J.G. Byrne, Transactions of Japan Institute of Metals, 9 (supplement) (1968) 514-520.
[15] D.L. Yin, K.F. Zhang, G.F. Wang, W.B. Han, Materials Science and Engineering A 392 (2005) 320–325.
[16] L. Guo, Z. Chen, L. Gao, Materials Science and Engineering A 528 (2011) 8537– 8545.
[17] A. Galiyev, R. Kaibyshev, G. Gottstein, Acta Materialia, 49 (2001) 1199–1207.
[18] T. Liu, F. Pan, X. Zhang, Materials and Design 43 (2013) 572–577.
[19] J.C. Oh, T. Ohkubo, T. Mukai, K. Hono, Scripta Materialia 53 (2005) 675–679.
[20] J.F. Nie, B.C. Muddle, Scripta Materialia, 37 (1997) 1475-1481.
[21] M.O. Pekguleryuz, E. Baril, Materials Transactions 42 (2001) 1258-1267.
[22] S.W. Xu, K. Oh-ishi, S. Kamado, F. Uchida, T. Homma, K. Hono, Scripta Materialia 65 (2011) 269–272.
[23] ASTM, ASTM Standards on Disc, Vol. 03.01, West Conshohocken, Philadelphia, 2003.
[24] A. Simar, Y. Bréchet, B.d. Meester, A. Denquin, T. Pardoen, Acta Materialia, 55 (2007) 6133–6143.
[25] J. Gil-Sevillano, Materials Science Forum, 113-115 (1993) 19-28.
[26] L.M. Cheng, W.J. Poole, J.D. Embury, D.J. Lloyd, Metallurgical and Materials Transactions A, 34 (2003) 2473-2481.
[27] J. Hirsch, T. Al-Samman, Acta Materialia, 61 (2013) 818–843.
[28] C.H. Cáceres, C.J. Davidson, J.R. Griffiths, C.L. Newton, Materials Science and Engineering A, 325 (2002) 344–355.
[29] X. Chen, F. Pan, J. Mao, J. Wang, D. Zhang, A. Tang, J. Peng, Materials and Design 32 (2011) 1526–1530.
[30] M. Vivas, P. Lours, C. Levaillant, A. Couret, M.-J. Casanove, A. Coujou, Philosophical Magazine A, 76 (1997) 921-931
[31] T. Liu, F. Pan, X. Zhang, Materials and Design 43 (2013) 572–577.
[32] H.-Y. Wu, F.-Z. Lin, Materials Science and Engineering A 527 (2010) 1194–1199.
[33] C.H. Cáceres, A.H. Blake, Materials Science and Engineering A 462 (2007) 193–196.
[34] P.B. Hirsch, F.J. Humphreys, Proceedings of the Royal Society of London A, 318 (1970) 45-72.
[35] D. Hull, D.J. Bacon, Introduction to Dislocations, Fifth ed., Elsevier Ltd., 2011.

Figure captions:

Fig. 1 Schematic illustration of the thermomechanical treatments practiced in this study: a) pre-deformation followed by precipitation hardening treatment at 250 °C, b) over-aging at 250 °C followed by deformation, c) pre-deformation, peak-aging at 250 °C followed by deformation, d) simultaneous deformation and precipitation and.

Fig. 2 A polarized optical micrograph showing the Mg-1 wt.% Ca alloy after homogenization treatment.

Fig. 3 Precipitation in Mg-1 wt.% Ca alloy: a) evolution of hardness in the course of precipitation hardening treatment at 250 °C, b) the effect of pre-deformation on precipitation hardening response of the material.

Fig. 4 TEM bright field images showing the Mg_2Ca precipitates in Mg-1Ca alloy after precipitation hardening treatment at 250 °C for 5 min: a) without pre-deformation, and b) with 5% pre-deformation at 100 °C. In both micrographs the electron beam is approximately parallel to $<11\bar{2}0>_{Mg}$. Arrows indicate the Mg_2Ca precipitates.

Fig. 5 Stress-true strain curves of the Mg-1 wt.% Ca alloy deformed at various precipitation states: a) over-aged, b) peak-aged, and c) under-aged.

Fig. 6 Mechanical properties of the Mg-1 wt.% Ca alloy at various precipitation state and thermomechanical treatments: a) 0.2% yield strength ($\sigma_{y0.2\%}$) and b) ultimate compressive strength.

Fig. 7 The work hardening behavior of the Mg-1 wt.% Ca alloy at various precipitation states and temperatures: a) over-aged, b) peak-aged and c) under-aged. The dashed guidelines show schematically how θ_0 is determined from the curves.

Fig. 8 Yield strength (proportionality limit) dependence of: a) work hardening rate and b) dynamic recovery rate of Mg-1 wt.% Ca alloy at various precipitation states at 250 °C.

Fig. 9 TEM bright field images showing the Mg_2Ca precipitates in the Mg-1Ca alloy after 30% deformation at 250 °C: a) under-aged, b) peak-aged and c) over-aged. In all images the electron beam is approximately parallel to $<11\bar{2}0>_{Mg}$. Arrows indicate the Mg_2Ca precipitates.

Fig. 10 TEM bright field images showing the deformed structure in a) under-aged and b) peak-aged Mg-1Ca alloy after 30% uni-axial compression at 250 °C.

Fig. 11 Temperature dependence of: a) work hardening rate and b) dynamic recovery rate of Mg-1 wt.% Ca alloy at various precipitation states.

Figure_1a
Click here to download high resolution image

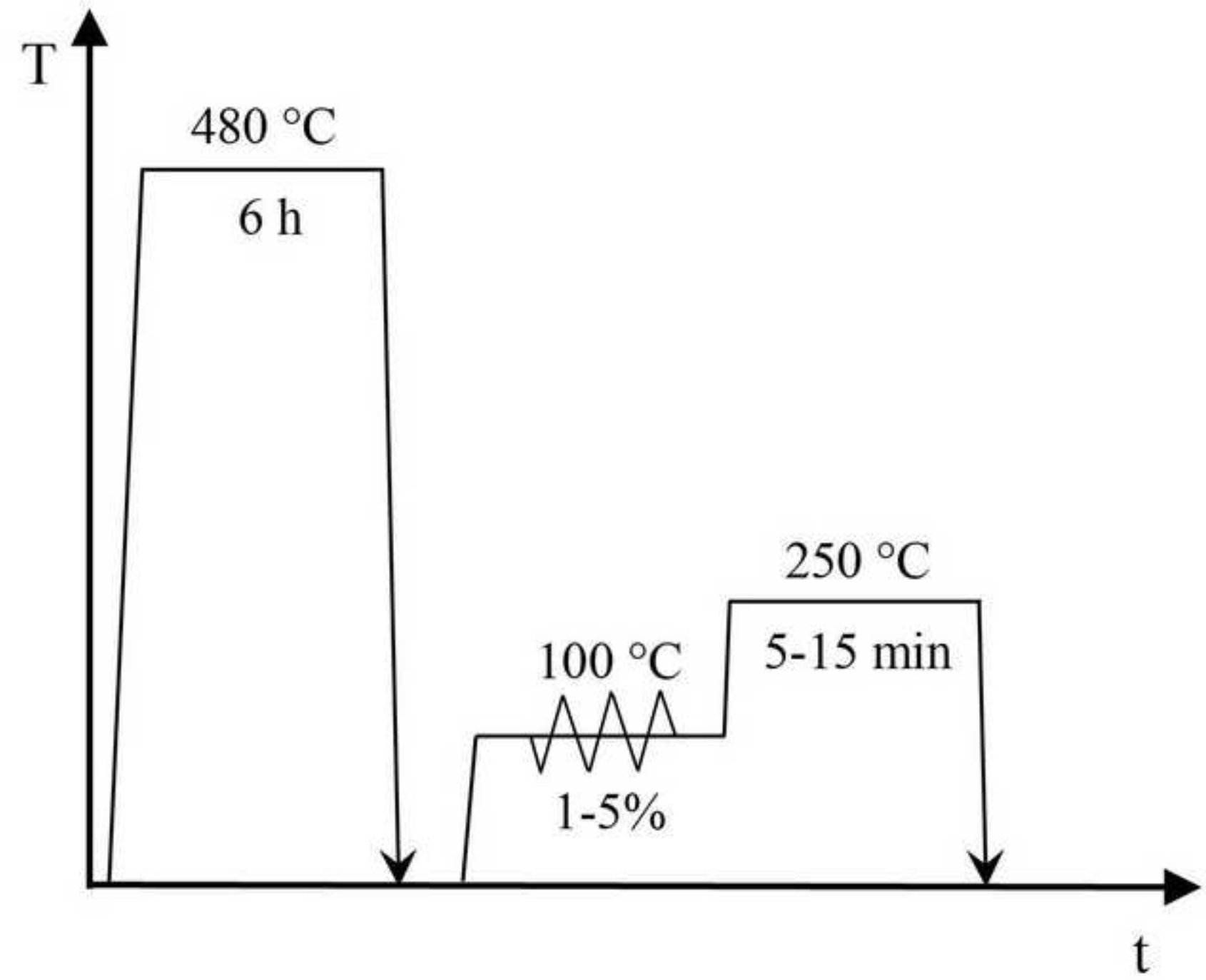

Figure_1b
Click here to download high resolution image

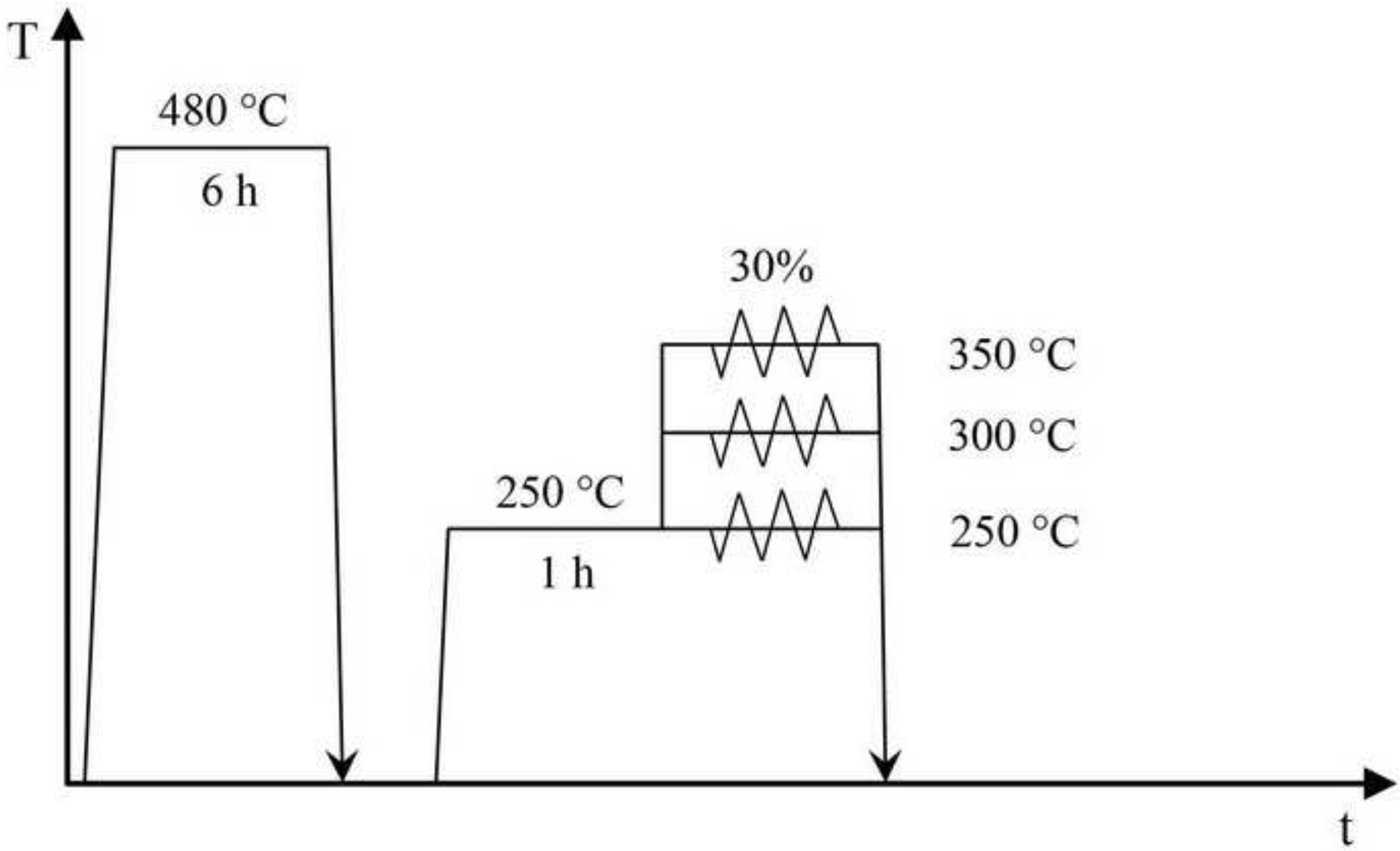

Figure_1c
Click here to download high resolution image

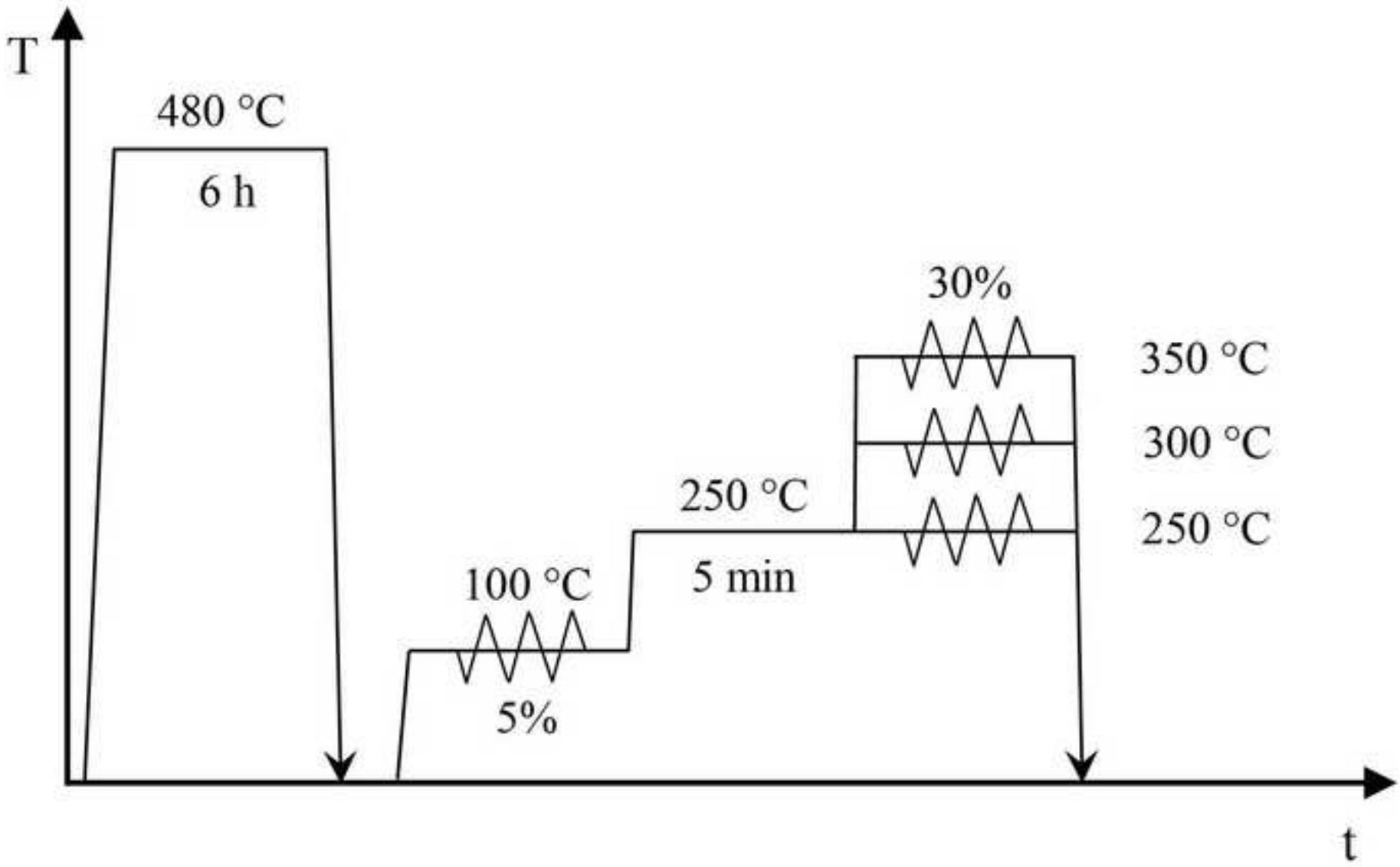

Figure_1d
Click here to download high resolution image

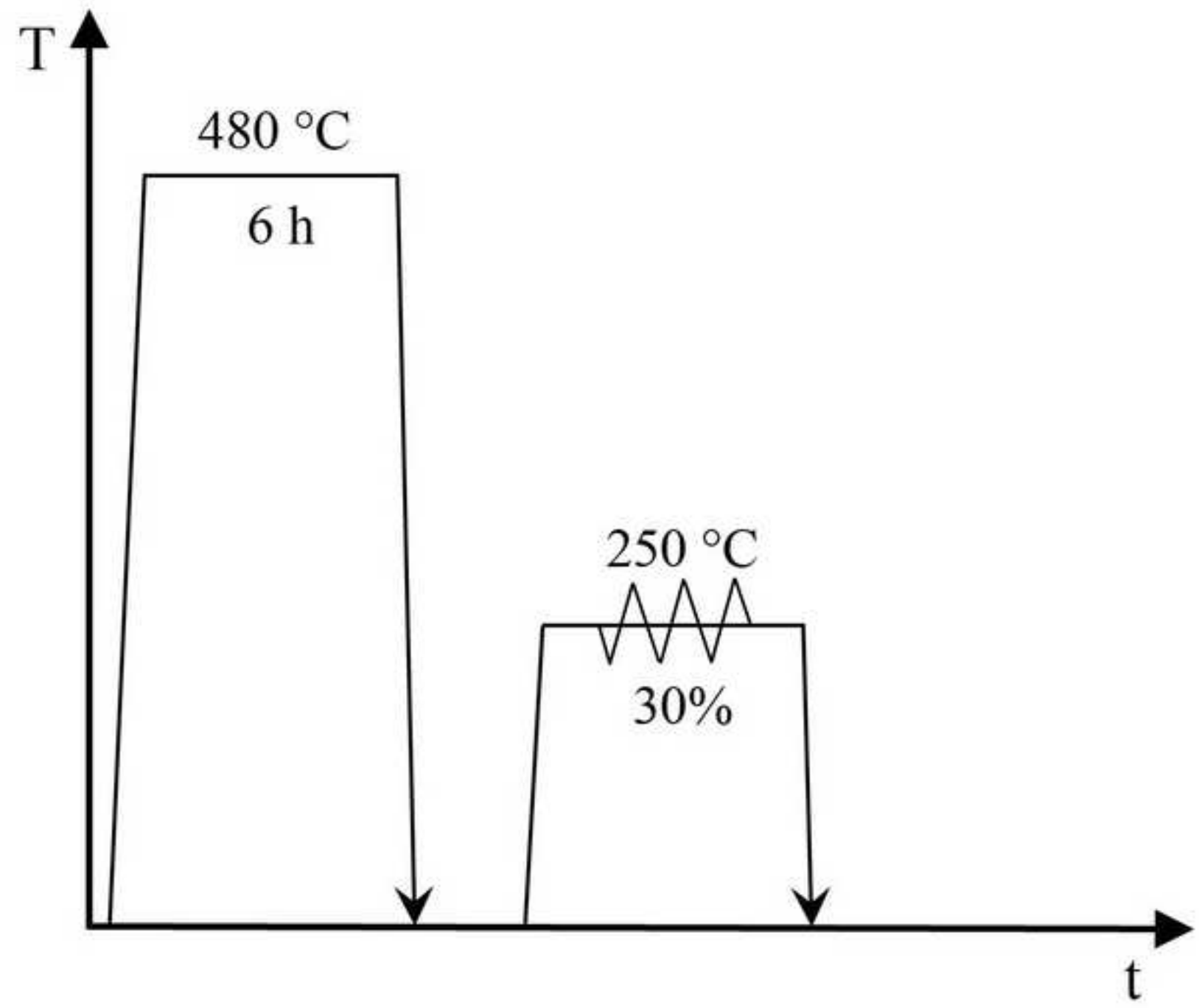

Figure_2
Click here to download high resolution image

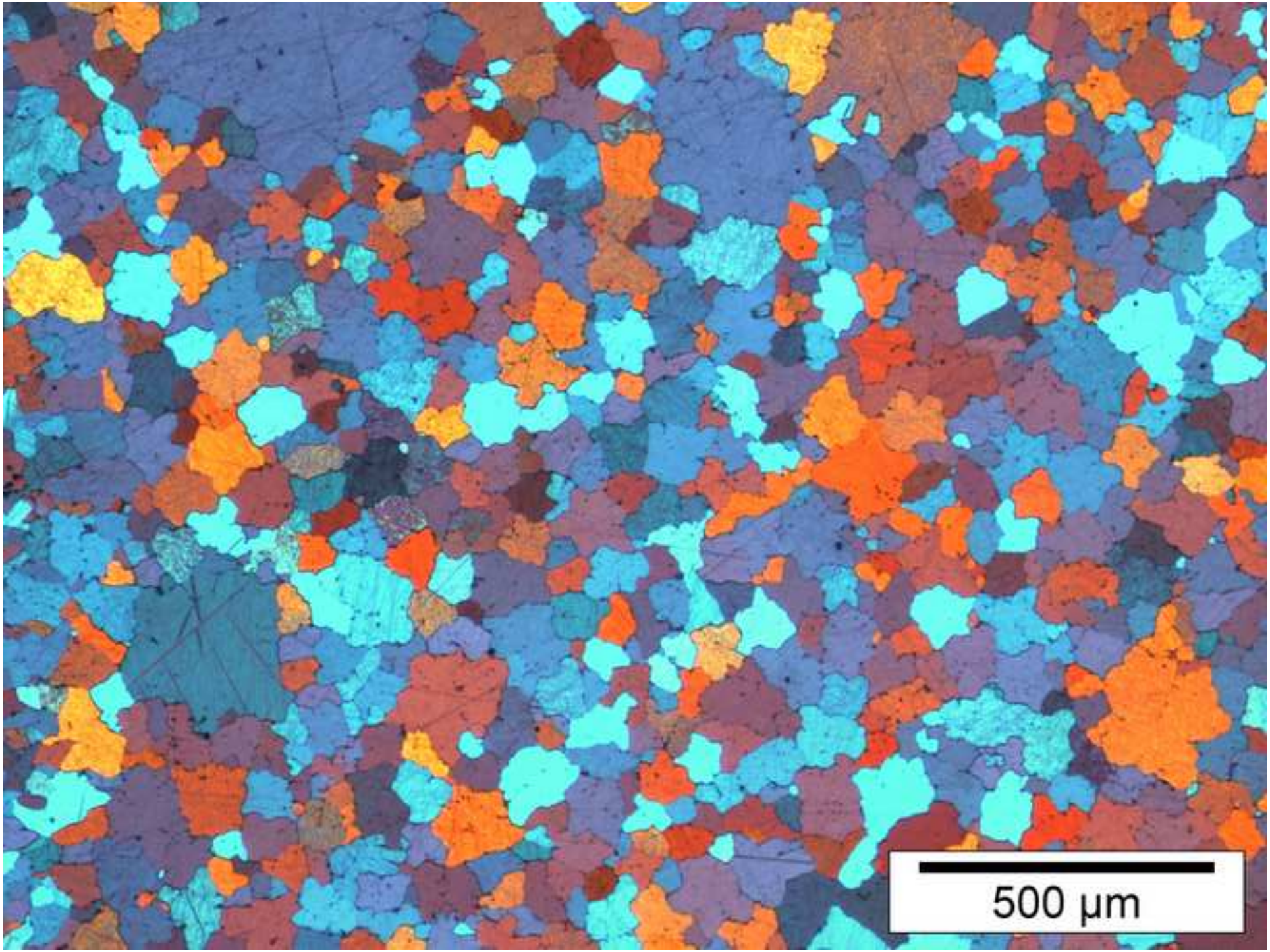

Figure_3a
Click here to download high resolution image

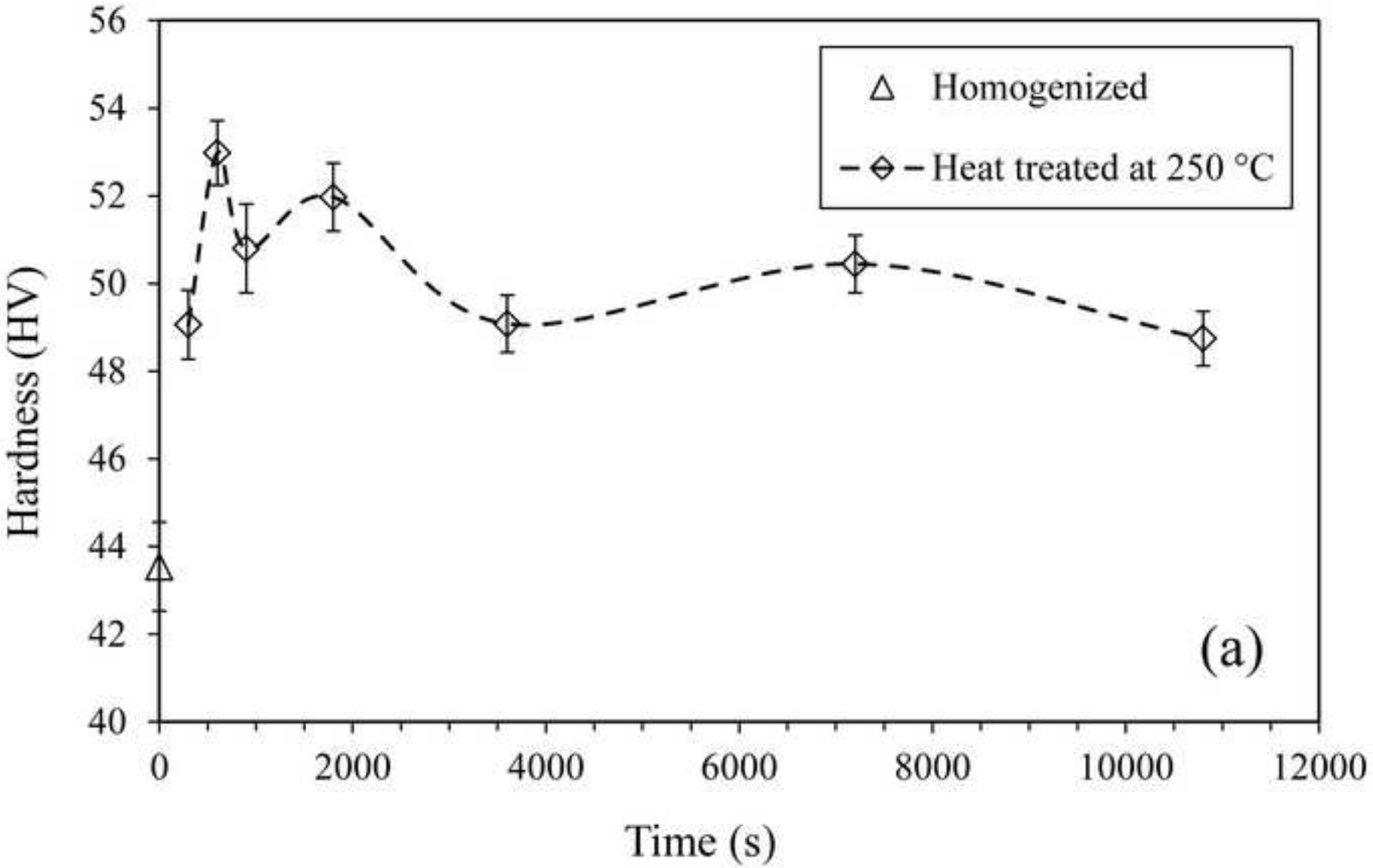

Figure_3b
Click here to download high resolution image

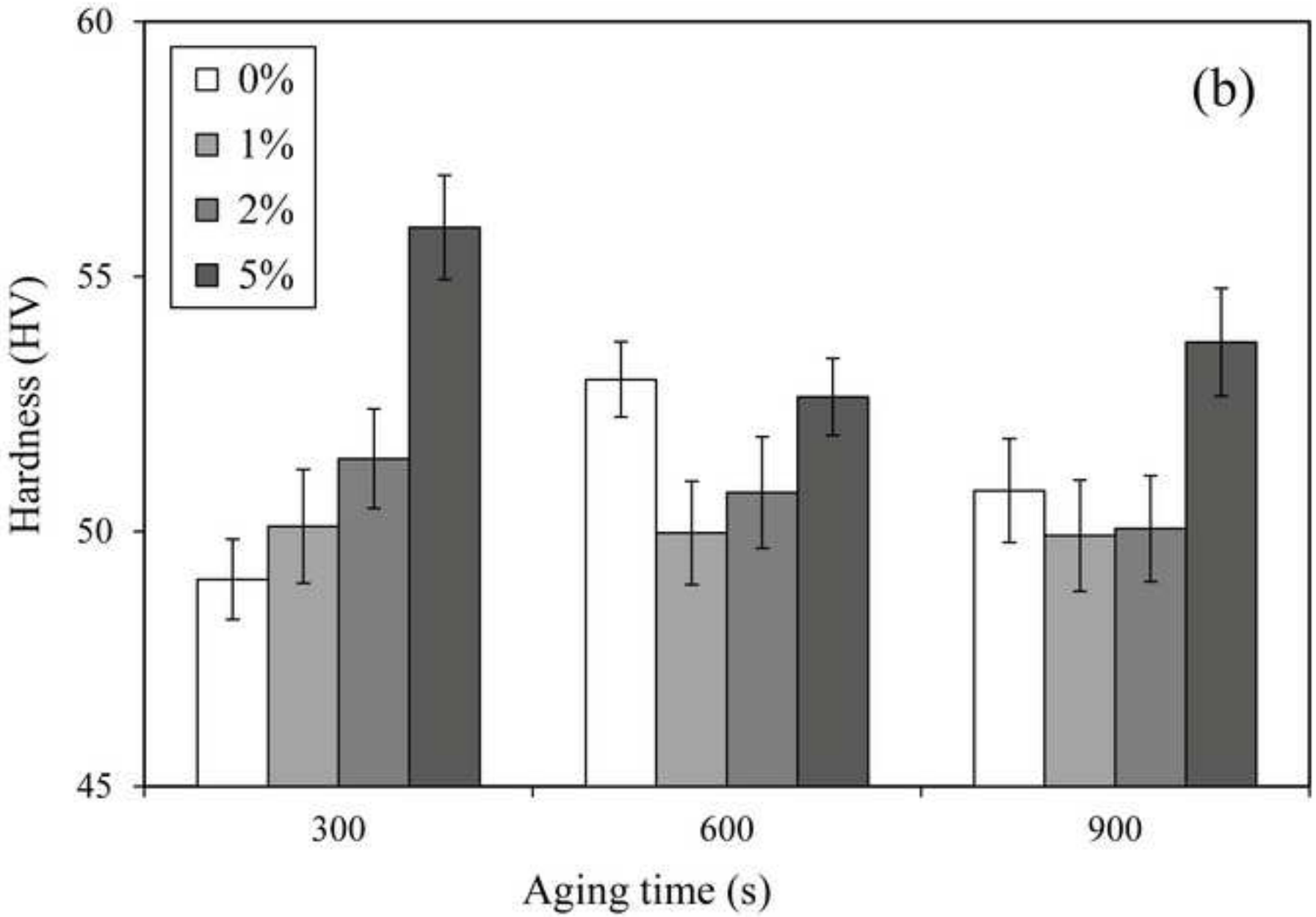

Figure_4a_02

Click here to download high resolution image

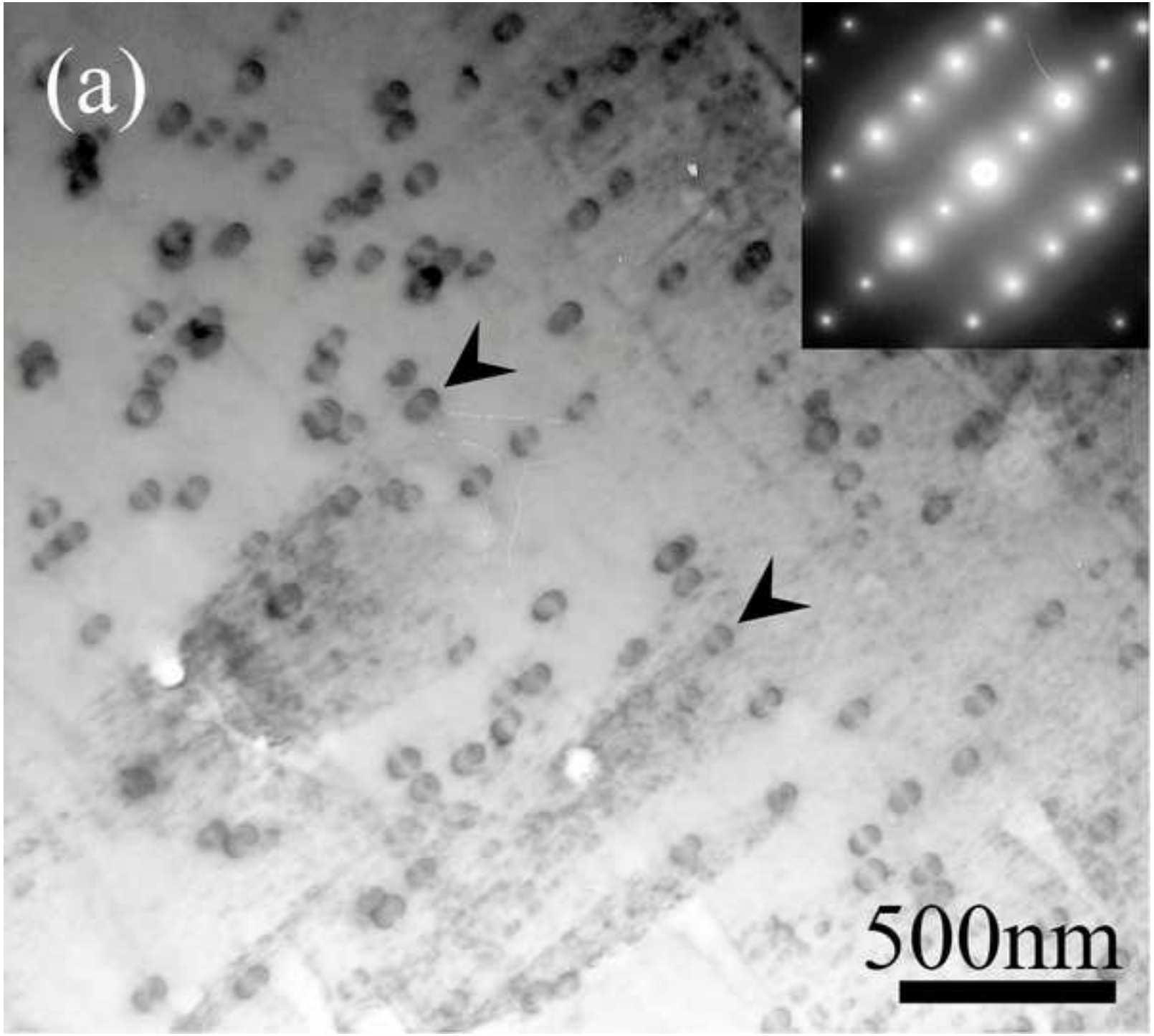

Figure_4b_02

Click here to download high resolution image

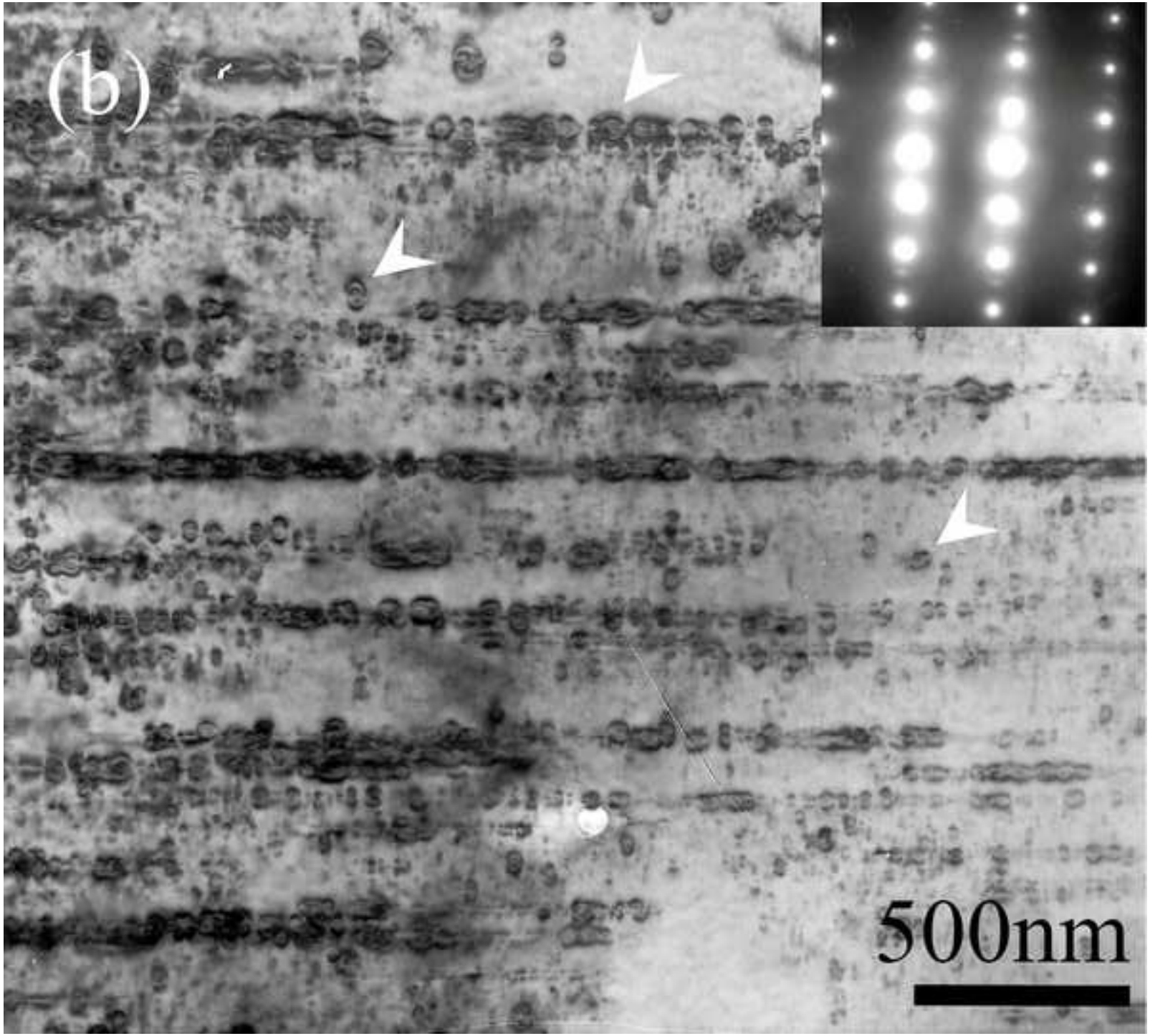

Figure_5
Click here to download high resolution image

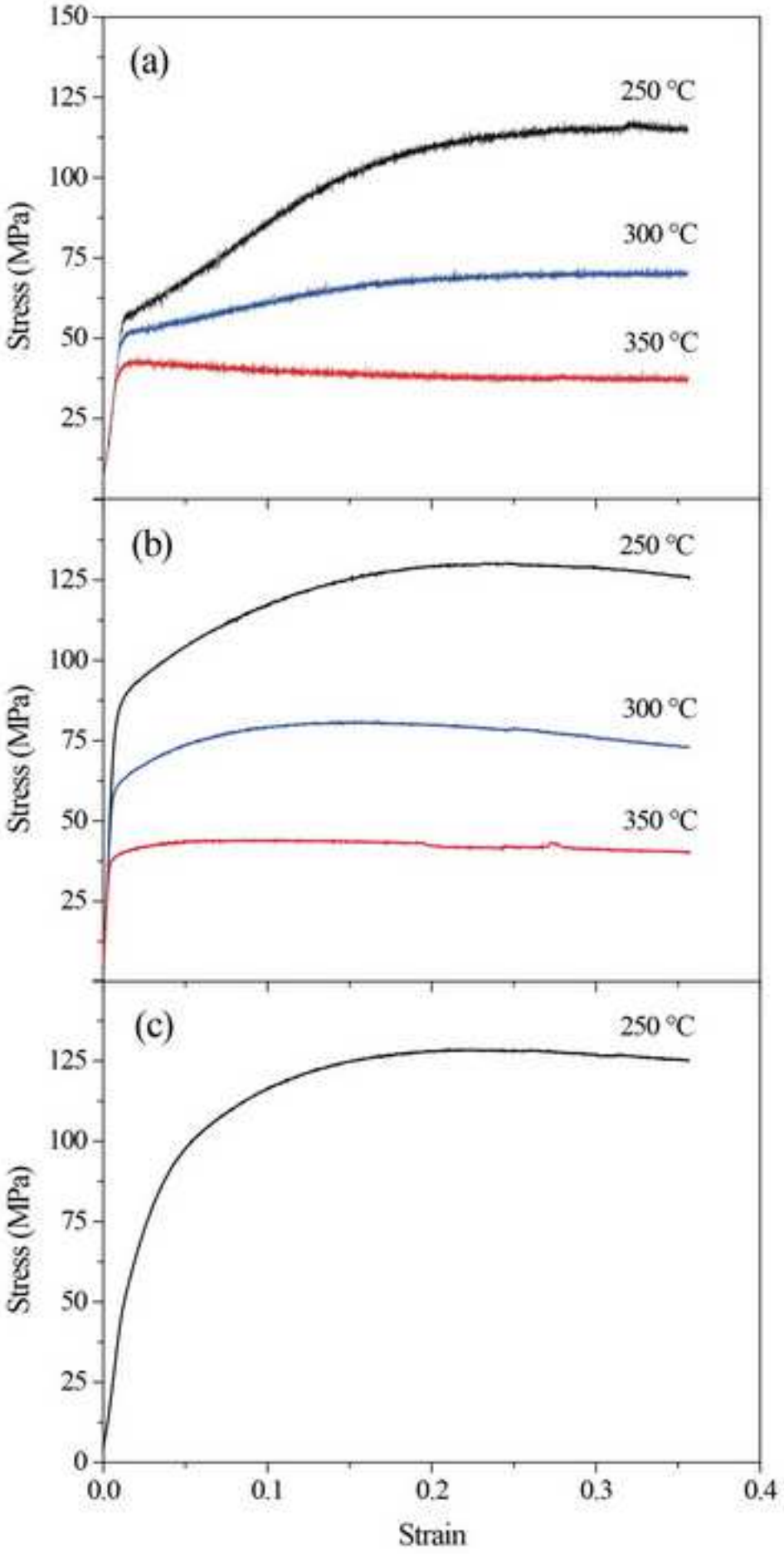

Figure_6
Click here to download high resolution image

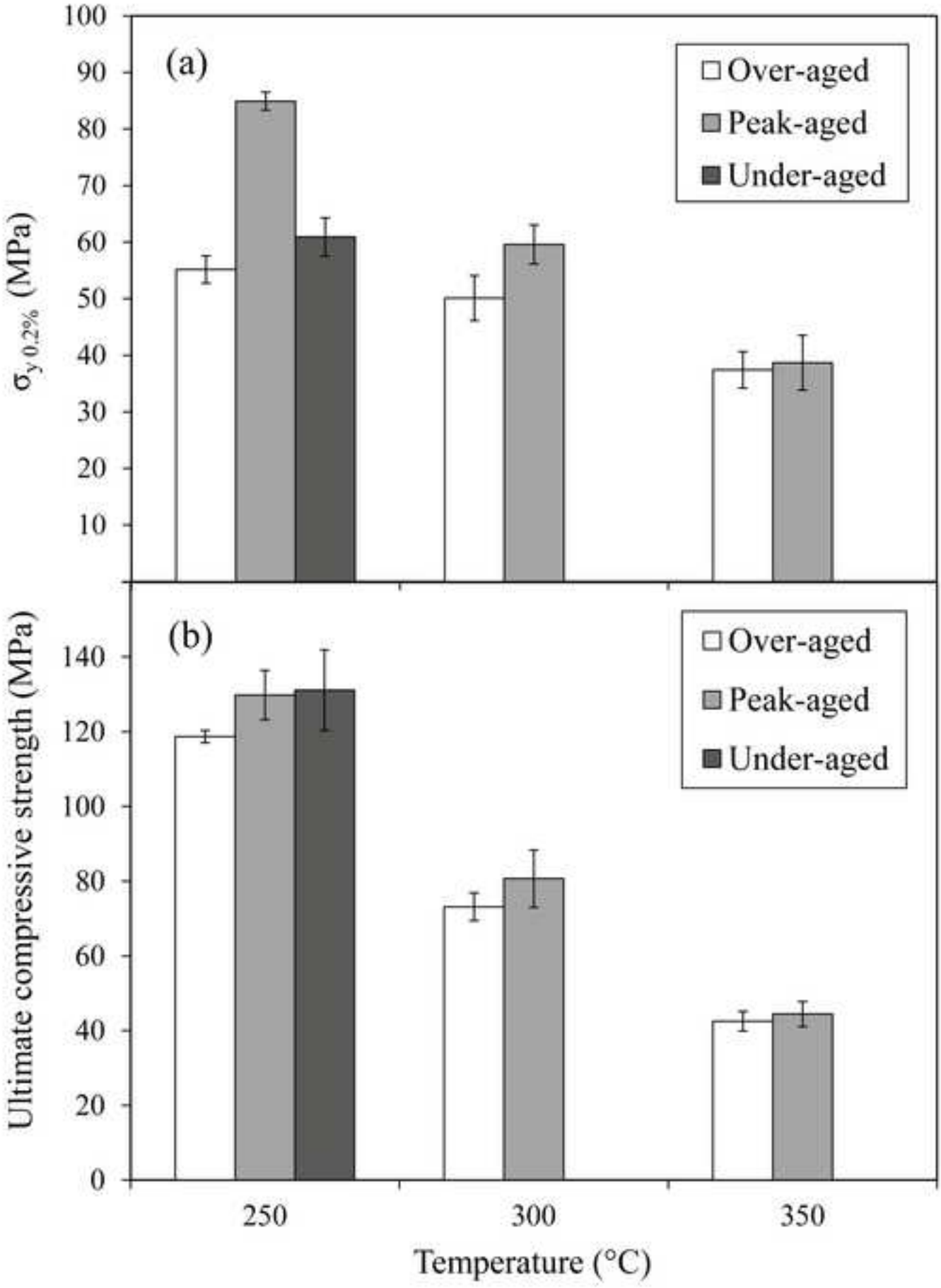

Figure_7_02
Click here to download high resolution image

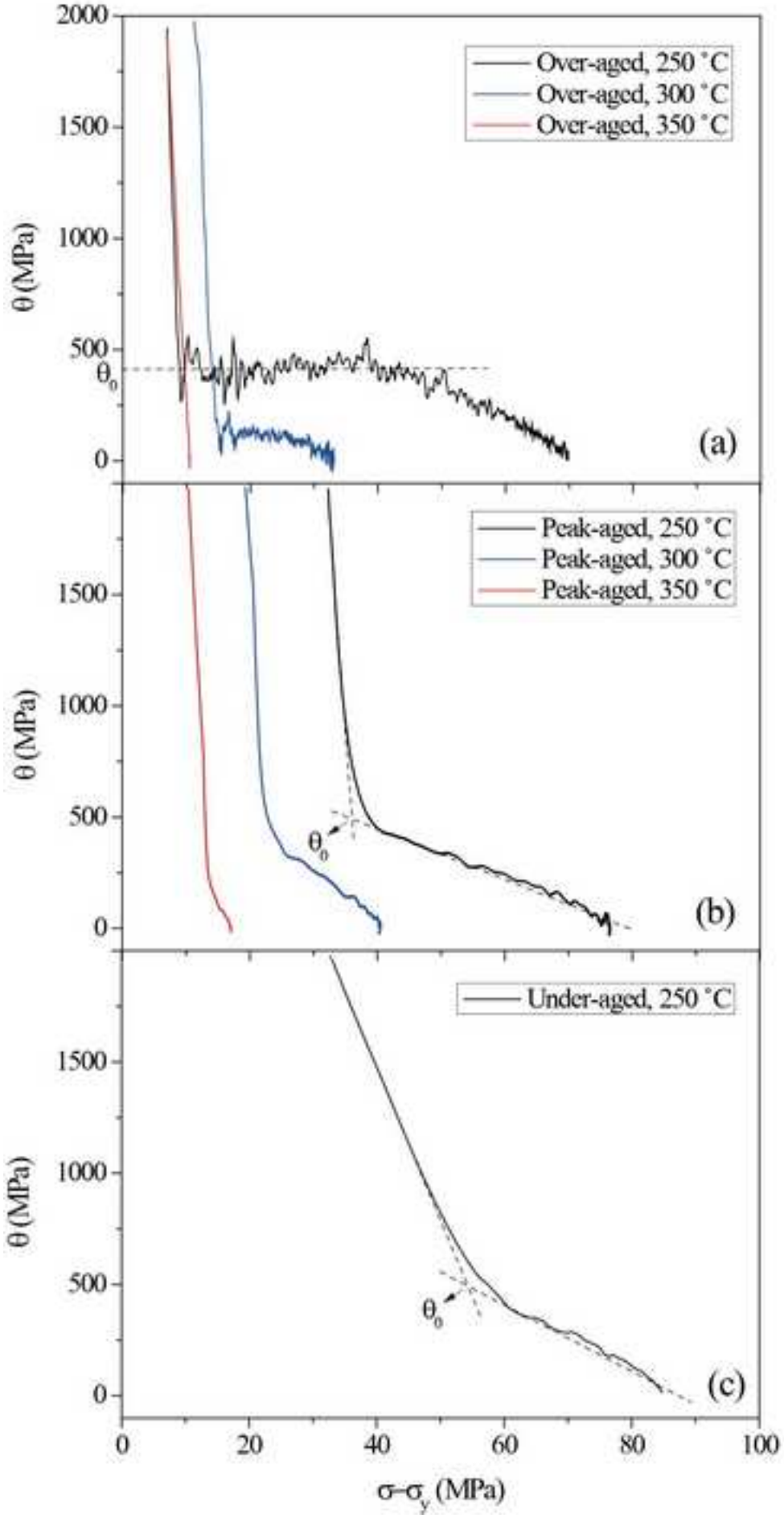

Figure_8
Click here to download high resolution image

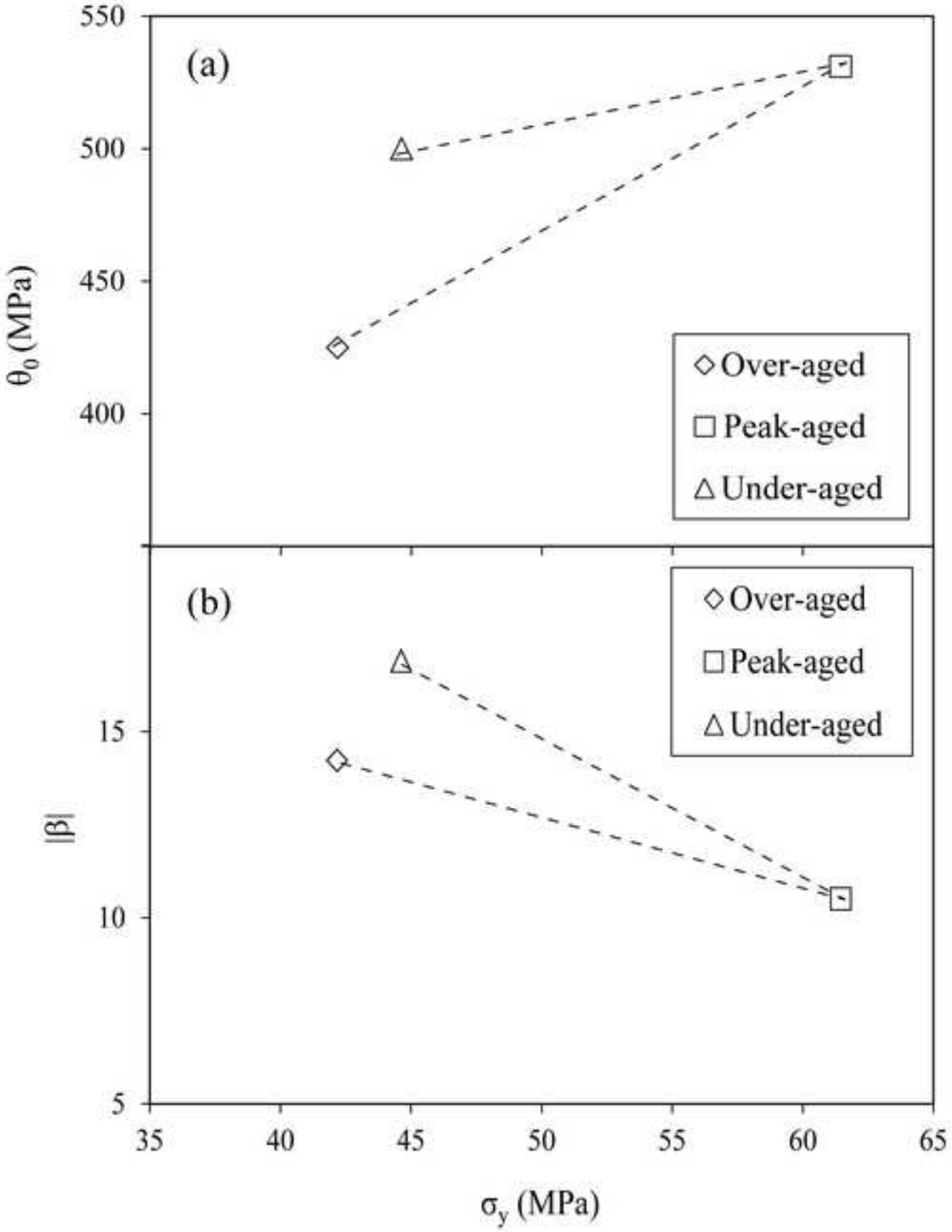

Figure_9a

Click here to download high resolution image

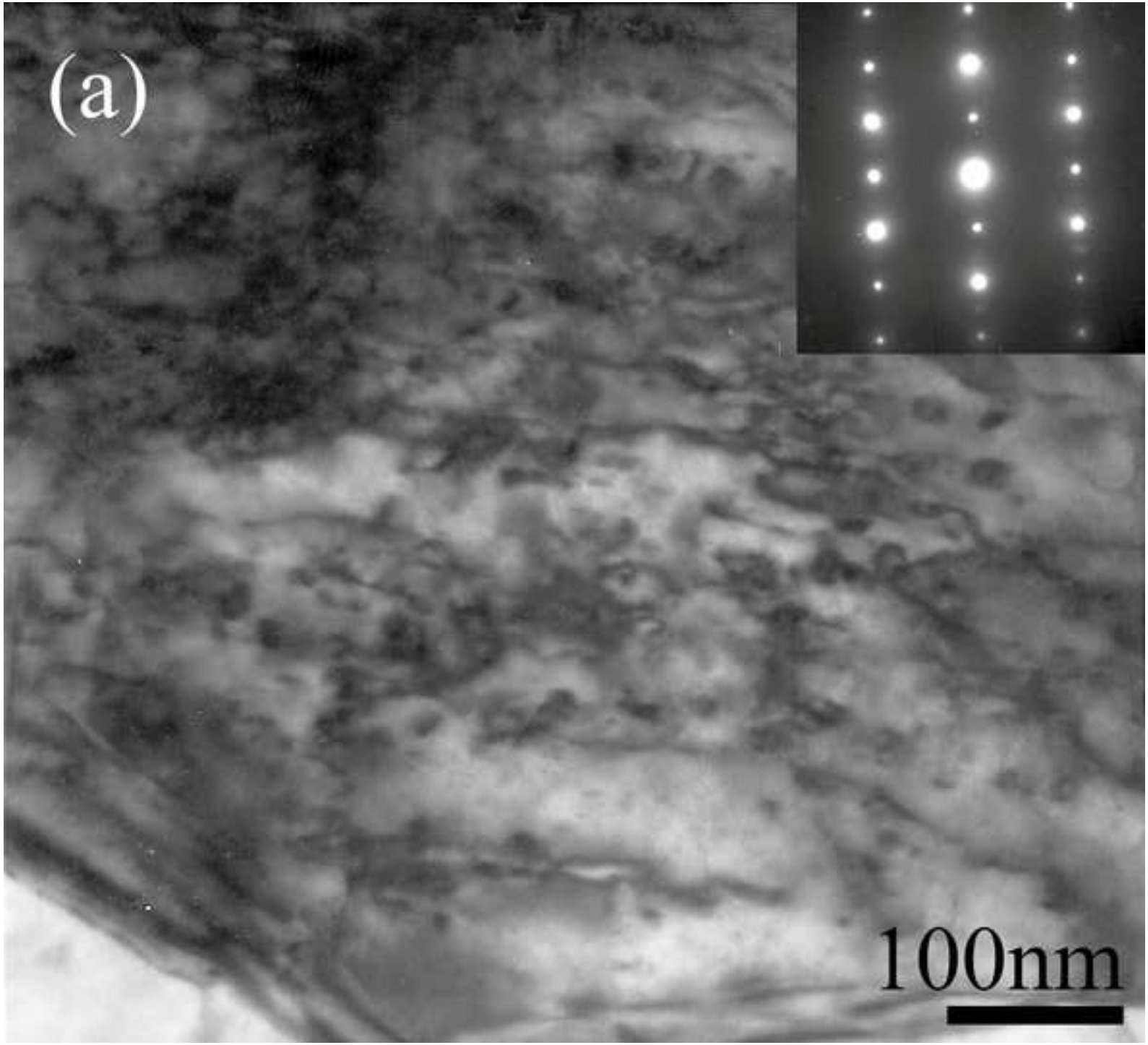

Figure_9b_02

Click here to download high resolution image

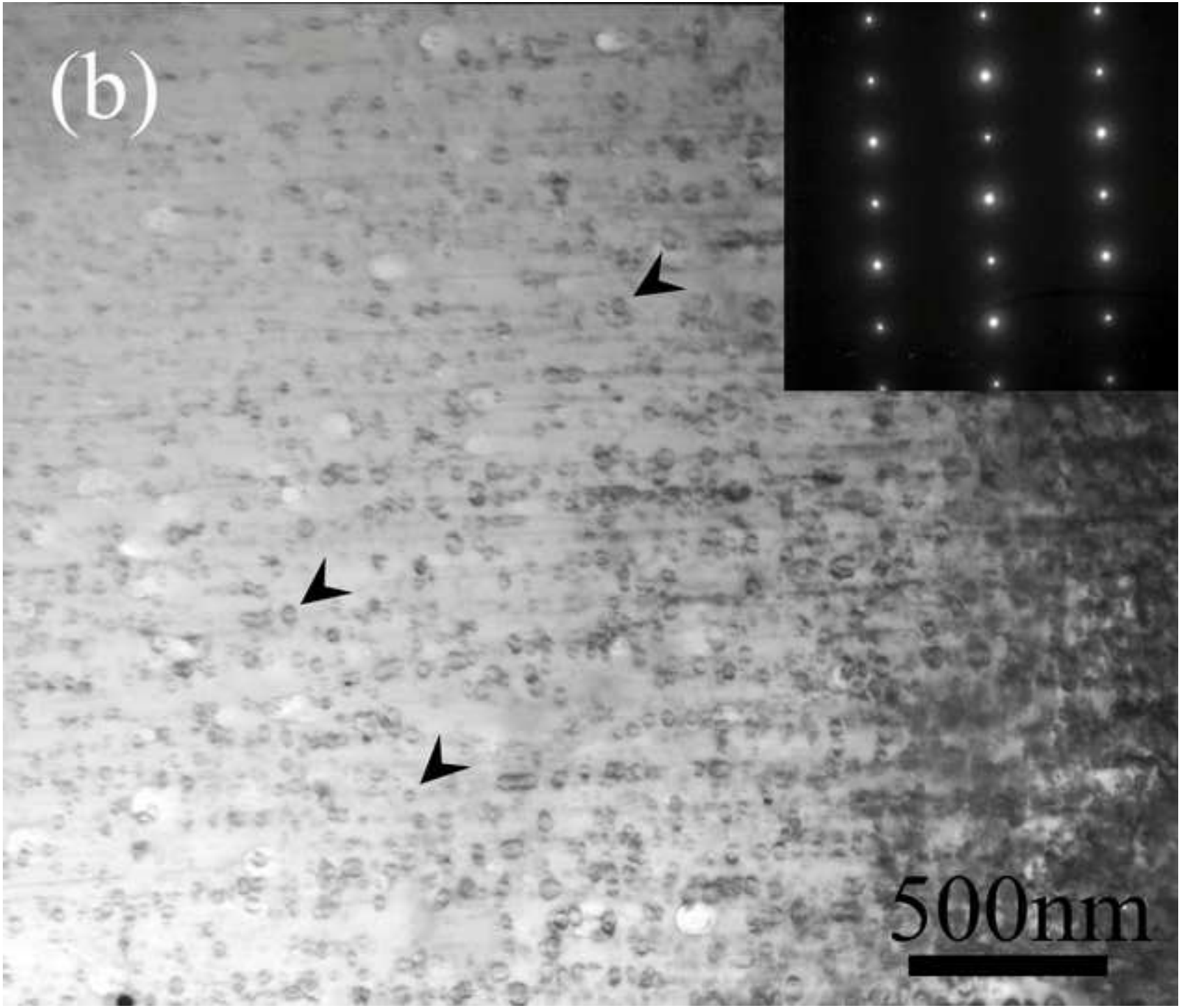

Figure_9c_02

Click here to download high resolution image

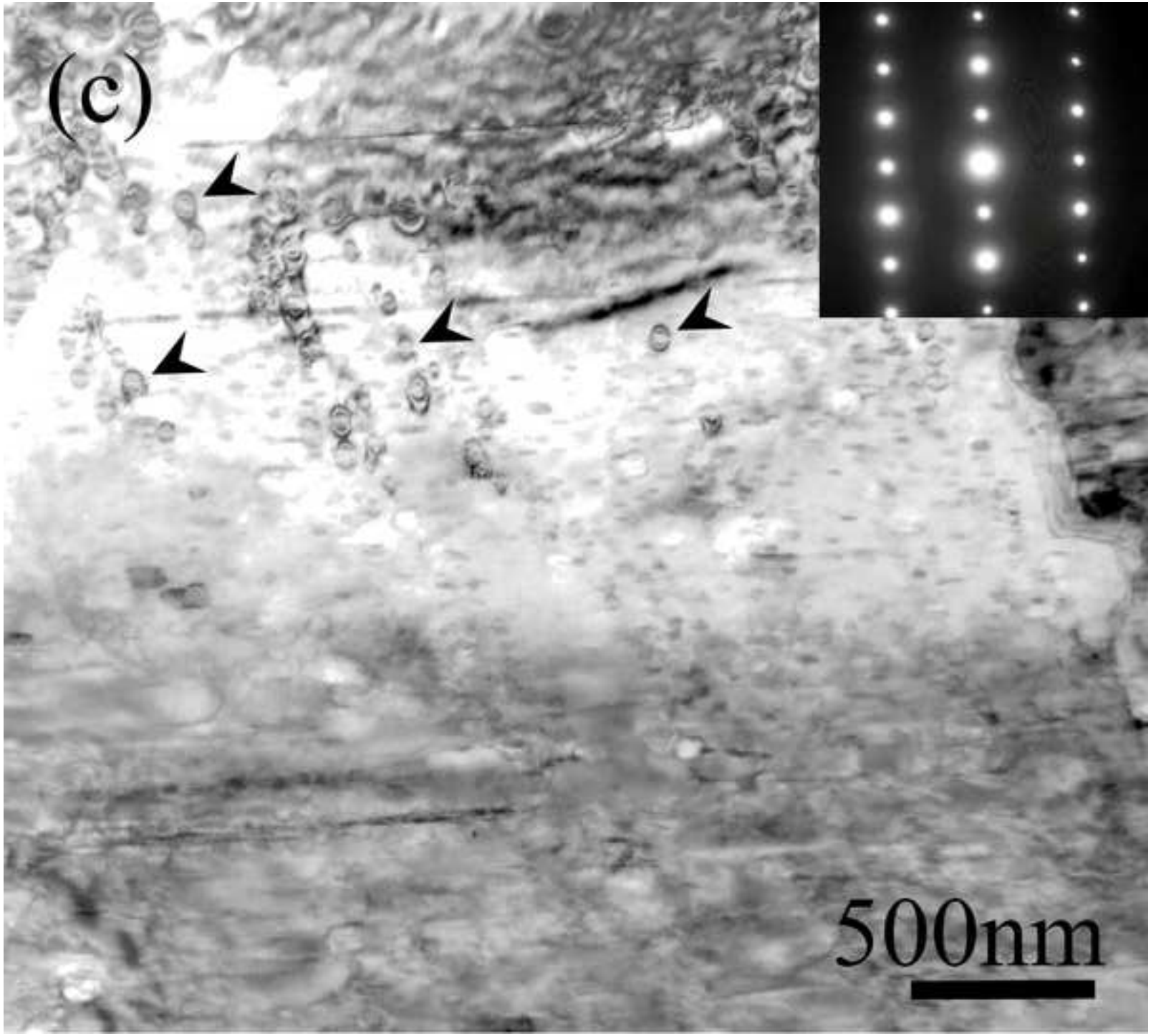

Figure 10a

Click here to download high resolution image

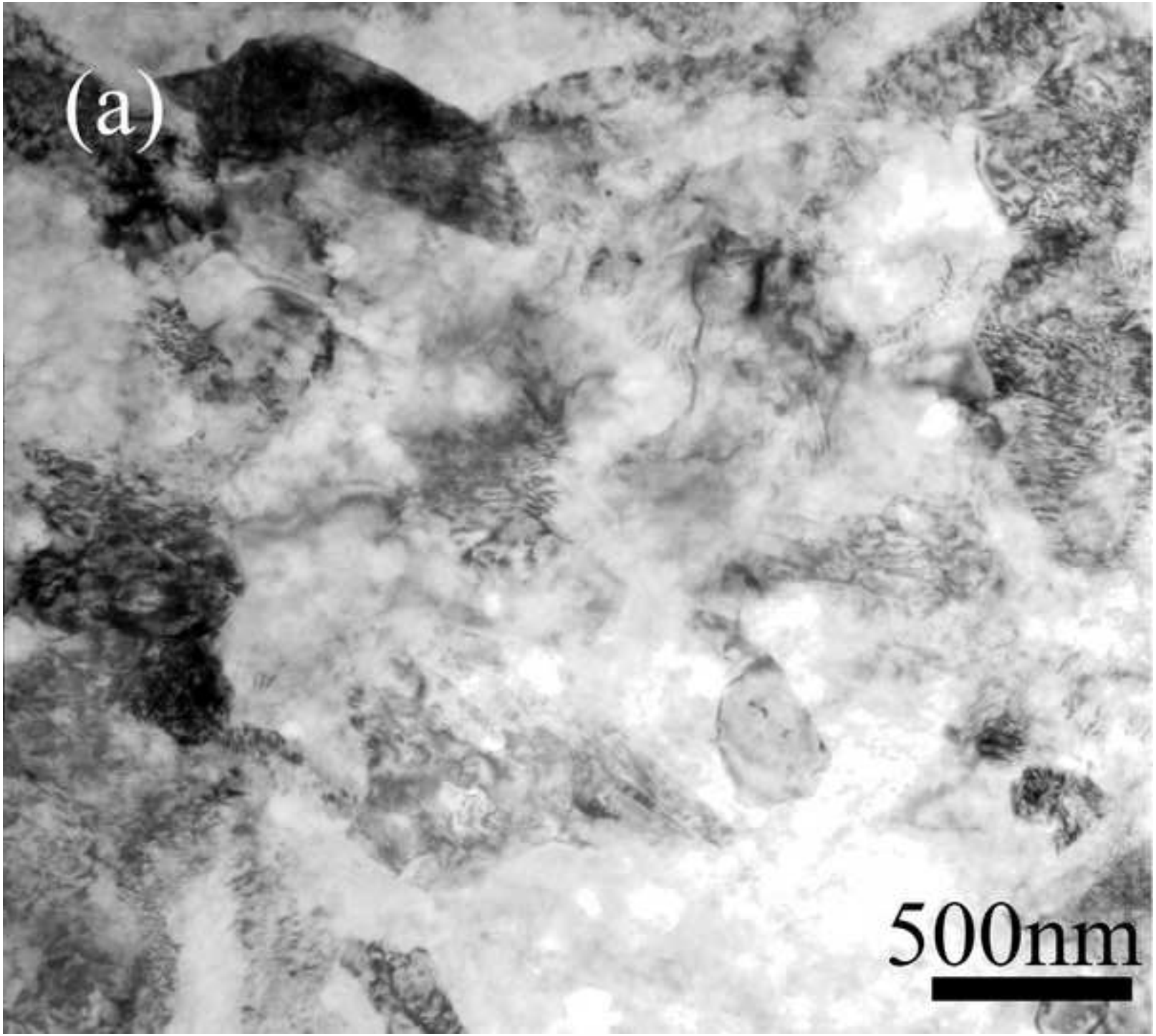

Figure 10b

Click here to download high resolution image

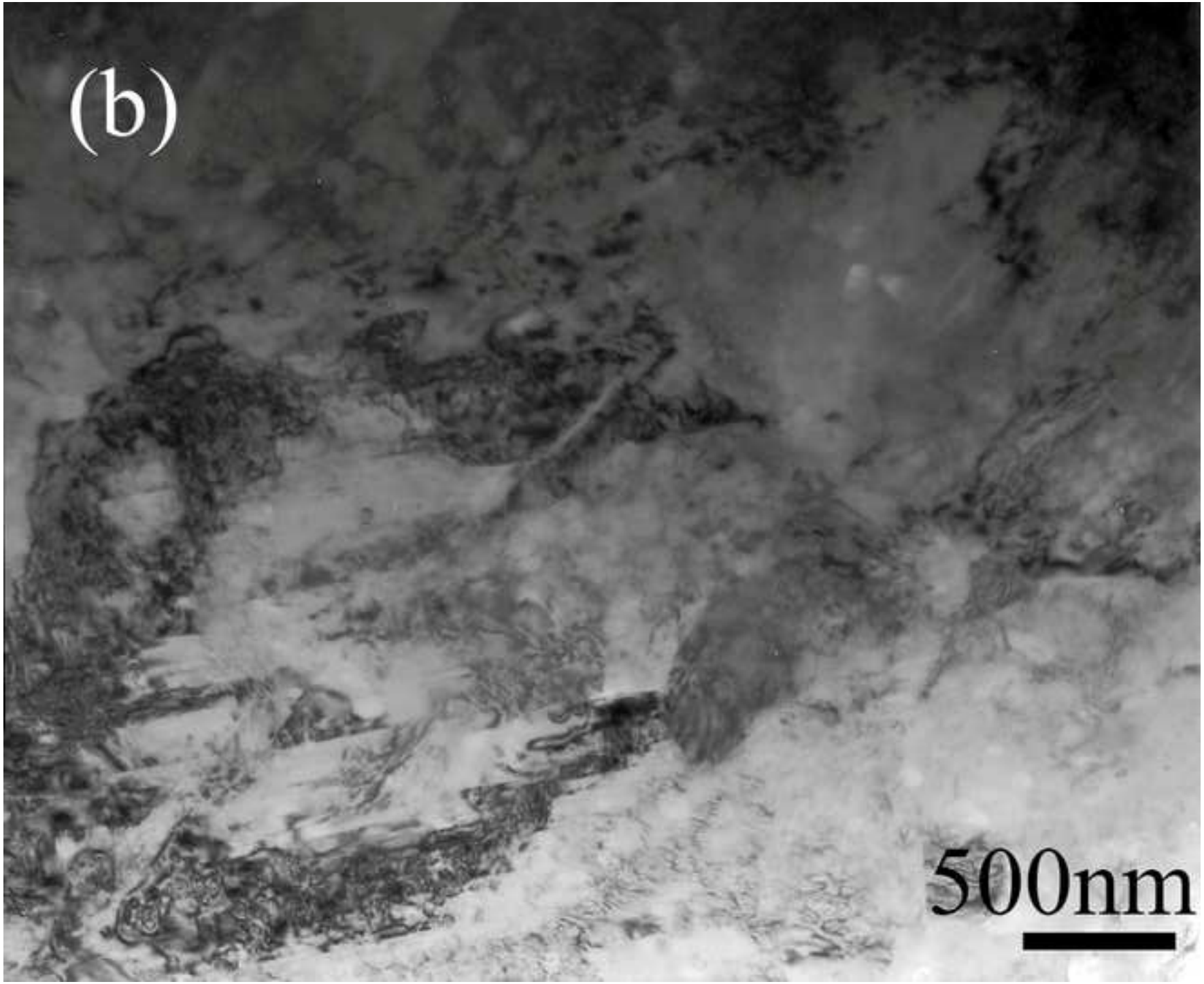

Figure_11
Click here to download high resolution image